direction of the minimum column density of galactic H I [$\sim 5 \times 10^{19}$ H I cm^{-2}, $\ell \sim 151.6°$, $b \sim 52.1°$ (*24*)], there is not a correspondingly high x-ray intensity. An emission measure of $\sim 1.3 \times 10^{-2}$ cm^{-6} pc would generate a count rate roughly three times what is observed in that direction. Because the two directions are not far from each other on the sky (~35°), this is difficult to reconcile in the case of an extensive x-ray halo. Second, the Draco nebula lies in the direction of a large complex of high-velocity clouds (HVCs) and it is possible that the background x-ray emission could be a relatively isolated phenomenon indicative of an interaction between the HVCs and the cooler gas in the galactic halo. Third, although the H I velocity information of the shadowing cloud strongly links the cloud to the Draco nebula, it will still be reassuring to have the distance confirmed by ISM absorption line measurements or the detection of shadowing by the rest of the Draco nebula.

This result illustrates the utility of ROSAT XRT/PSPC observations in a search for SXRB shadowing. Any discrete absorbing feature with a known distance is a target for such a search, and the observed flux can be divided into foreground and background emission. With a sufficient number of targets, we can bypass both the displacement model and interspersed model with their limitations of treating only the general appearance of the SXRB and map out in detail the distribution of x-ray emission in the solar neighborhood. This same analysis can be extended to the higher energy M band (0.5 to 1.0 keV) and greater sample distances from the sun (~1 kpc in the galactic plane). One caveat, however, is that, although ROSAT survey data are in general usable in the search for C band shadows if an accuracy of 5 to 10% in the fraction determination is sufficient, a search for M band shadows will require the greater exposure of a pointed observation.

REFERENCES AND NOTES

1. C. S. Bowyer, G. B. Field, J. E. Mack, *Nature* **217**, 32 (1968).
2. A. N. Bunner, *et al.*, *ibid.* **223**, 1222 (1969).
3. F. J. Marshall and G. W. Clark, *Astrophys. J.* **287**, 633 (1984).
4. D. McCammon, D. N. Burrows, W. T. Sanders, W. L. Kraushaar, *ibid.* **269**, 107 (1983).
5. S. L. Snowden, D. P. Cox, D. McCammon, W. T. Sanders, *ibid.* **354**, 211 (1990).
6. P. Jakobsen and S. M. Kahn, *ibid.* **309**, 682 (1986).
7. W. Hirth, U. Mebold, M. Dahlem, P. Müller, *Astrophys. Space Sci.*, in press.
8. D. McCammon, A. N. Bunner, P. L. Coleman, W. L. Kraushaar, *Astrophys. J.* **168**, L33 (1971).
9. D. McCammon, S. S. Meyer, W. T. Sanders, F. O. Williamson, *ibid.* **209**, 46 (1976).
10. D. N. Burrows, D. McCammon, W. T. Sanders, W. L. Kraushaar, *ibid.* **287**, 208 (1984).
11. J. Trümper, *Adv. Space Res.* **2**, 241 (1983).
12. B. Aschenbach, *Appl. Opt.* **27** (no. 8), 1404 (1988).
13. E. Pfeffermann *et al. Proc. SPIE Int. Soc. Opt. Eng.* **733**, 519 (1987).
14. D. Lilienthal, A. Wennmacher, U. Herbstmeier, U. Mebold, *Astron. Astrophys.*, in press.
15. S. L. Snowden and P. P. Plucinsky, in preparation.
16. W. Goerigk, U. Mebold, K. Reif, P. M. W. Kalberla, L. Velden, *Astron. Astrophys.* **120**, 63 (1983).
17. P. M. W. Kalberla, U. Mebold, W. Reich, *ibid.* **82**, 275 (1980).
18. U. Herbstmeier, R. Rohlfs, U. Mebold, in *The Physics and Chemistry of Interstellar Molecular Clouds*, G. Winnewisser and J. T. Armstrong, Eds. (Lecture Notes in Physics No. 331, Springer-Verlag, Berlin, 1989), p. 195.
19. A. Heithausen and U. Mebold *Astron. Astrophys.* **214**, 347 (1989).
20. U. Herbstmeier, thesis, Universität Bonn (1990).
21. J. C. Raymond, in *Hot Thin Plasmas in Astrophysics*, R. Pallavicini, Ed. (Kluwer Academic, Dordrecht, 1988), p. 3.
22. R. Morrison and D. McCammon, *Astrophys. J.* **270**, 119 (1983).
23. M. Lampton, B. Margon, S. Bowyer, *ibid.* **208**, 177 (1976).
24. K. Jahoda, F. J. Lockman, D. McCammon *ibid.* **354**, 184 (1990).

25. We thank B. Wakker for providing the IRAS 100-μm map corrected for scanning effects. We also acknowledge useful discussions with K. Jahoda, D. McCammon, and W. Sanders. This work was supported in part by the Max Planck Institute for Extraterrestrial Physics, the National Aeronautics and Space Administration under grants NAG 5-1438 and NAG 5-629, and the Deutsche Forschungsgemeinschaft under grant ME 745/7-2.

11 April 1991; accepted 2 May 1991

Crystallinity of the Double Layer of Cadmium Arachidate Films at the Water Surface

F. LEVEILLER, D. JACQUEMAIN, M. LAHAV, L. LEISEROWITZ, M. DEUTSCH, K. KJAER, J. ALS-NIELSEN

A crystalline counterionic layer at the interface between an electrolyte solution and a charged layer of insoluble amphiphilic molecules was observed with grazing incidence synchrotron x-ray diffraction. Uncompressed arachidic films spread over 10^{-3} molar cadmium chloride solution (pH 8.8) spontaneously form crystalline clusters with coherence lengths of ~1000 angstroms at 9°C. Ten distinct diffraction peaks were observed, seven of which were attributed to scattering only from a crystalline Cd^{2+} layer and the other three to scattering primarily from the arachidate layer. The reflections from the Cd^{2+} layer were indexed according to a 2 × 3 supercell of the arachidate lattice with three Cd^{2+} ions per cadmium unit cell.

THE INTERFACIAL REGION BETWEEN a charged surface and an electrolyte is central to many processes such as those occurring during electrodeposition, ion transport through biological membranes, preparation of Langmuir-Blodgett films (*1*), biomineralization (*2*), and induced oriented nucleation of inorganic systems (*3*) under Langmuir monolayers. The use of direct methods such as grazing incidence x-ray diffraction (GID) and specular x-ray reflection (XR), when applied to films spread on the surface of liquids, has demonstrated that the surfactant molecules can acquire in-plane long-range order (*4–6*) and that metal ions, when present in solution, interact closely with the charged monolayer head groups at the interface (*7*). However, it was not known whether the ion distribution near such charged, ordered surfaces may be crystalline, particularly if the monolayer is singly charged and the counterion doubly charged (*8, 9*). In such a system, a monolayer not fully ionized may induce short-range order of the counterionic layer with the possibility of an incommensurate structure to meet charge neutrality. On the other hand, if the monolayer is fully ionized, the counterionic layer may still be incommensurate with that of the monolayer or may be arranged in a supercell.

X-ray standing waves were recently used to demonstrate that the Zn^{2+} double layer at a phospholipid membrane–aqueous interface is diffuse (*10*). Liquid-surface extended x-ray absorption fine structure (EXAFS) spectroscopy experiments on manganese stearate films (*11*) at room temperature yielded a Mn–Mn nearest neighbor distance at the surface in the compressed phase only, indicating at least short-range order. GID measurements of lead arachidate (*5*) monolayers at room temperature gave no indication of ordering of the Pb^{2+} ions. Here we describe a GID study of uncompressed cadmium arachidate monolayers at 9°C, which demonstrates the presence of an ordered Cd counterionic layer of a unit cell commensurate with, but larger than, that of the arachidate monolayer.

For these measurements we used the liquid-surface diffractometers on the wiggler

F. Leveiller, D. Jacquemain, M. Lahav, L. Leiserowitz, Structural Chemistry Department, Weizmann Institute of Science, Rehovot 76100, Israel.
M. Deutsch, Physics Department, Bar-Ilan University, Ramat-Gan 52100, Israel.
K. Kjaer and J. Als-Nielsen, Physics Department, Risø National Laboratory, DK4000 Roskilde, Denmark.

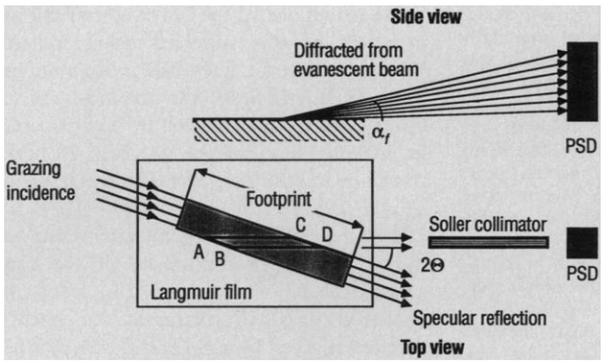

Fig. 1. Top and side views of the GID geometry. The footprint of the grazing incidence beam is indicated by the darker area. The position-sensitive detector (PSD) has its axis along the vertical direction (z). Only the area ABCD contributes to the measured scattering.

beam line W1 and on the bending magnet beam line D4 at Hasylab, Deutsche Electron Synchrotron (DESY), Hamburg. A sealed and thermostated Langmuir trough equipped with a Wilhelmy balance was mounted on the diffractometer, the geometry of which (*12*) is shown schematically in Fig. 1. Arachidic acid, $C_{19}H_{39}CO_2H$, was spread at 20°C over a $CdCl_2$ subphase (10^{-3} M) adjusted to a pH of about 8.8 by the addition of ammonia (NH_3) (*13*). A diffraction peak at q_x = 1.599 Å^{-1} was then monitored (*14*) upon reduction of temperature. It started forming at about 12°C and became sharp and intense upon further reduction of the temperature, signifying an increase of crystalline order (Fig. 2). This crystallinity may have been induced by removal of the rotational disorder of the molecular chains of the monolayer upon reduction of temperature, as was indicated by GID studies of fatty acid and alcohol monolayers (*15–17*) over water in the range 12° to 1°C. We set the subphase temperature in the trough at 9°C before recording the GID spectra. We reduced the background level during measurements considerably by maintaining a He atmosphere inside the trough.

For an uncompressed monolayer at a surface pressure π = 0 mN m^{-1} and 67% surface coverage (28 Å^2 per molecule), no less than ten distinct in-plane diffraction peaks were observed in the range measured, 0.470 Å^{-1} ≤ q_x ≤ 1.714 Å^{-1} (Fig. 3B). The strongest peaks around q_x = 1.5 Å^{-1} yield crystalline coherence lengths (*18, 19*) ~1000 Å, close to the resolution limit. By contrast, over pure water under similar conditions, a relatively weak peak at q_x = 1.441 Å^{-1} was detected (Fig. 3D, left), yielding a crystalline coherence length of only 500 Å. Thus, the presence of Cd^{2+} ions in the subphase promotes the crystalline self-aggregation of the monolayer.

The x-ray pattern of uncompressed cadmium arachidate is interpreted as follows: The three intense peaks in the range 1.5 Å^{-1} ≤ q_x ≤ 1.7 Å^{-1}, denoted the "triplet," are attributable to ordering of the arachidate molecules. This is clearly demonstrated by their Bragg rod profiles (*6, 20–22*) (Fig. 3A), which have a full width at half maximum FWHM(q_z) of 0.25 Å^{-1}, corresponding to a molecular length of about 25 Å, which indicates a contribution from the hydrocarbon backbone. By contrast, the profiles of the remaining reflections are flat to beyond 0.8 Å^{-1}, as exemplified in Fig. 3A by the Bragg rod of the peak at q_x = 1.284 Å^{-1} (Fig. 3B) indicating a contribution from a thin layer of scattering atoms of thickness (*23*) at most 4 Å and thus not from the arachidate molecules (*24*). The Bragg rod profiles attributable to the arachidate molecules (Fig. 3A) exhibit maxima in q_z at 0.2 to 0.3 Å^{-1}, from which we deduce (*6, 22*) a tilt angle from the vertical of ~11° of the molecular chains between next nearest neighbors (*25*) in a plane almost perpendicular to the a axis.

The reflections (Table 1) of the "triplet" with d spacings of 4.18, 4.13, and 3.93 Å were assigned $\{h,k\}$ indices (*26*) of $\{0,1\}$, $\{1,\bar{1}\}$, and $\{1,0\}$, respectively, to yield an oblique cell with lattice parameters a = 4.60 Å, b = 4.89 Å, γ = 121.3° with an area of 19.2 Å^2. For comparison, compressed arachidic acid over pure water at 9°C yields a "doublet" with $d_{1\bar{1}} = 3.82$, $d_{10} = d_{01} = 4.19$ Å (Fig. 3D, right), from which a distorted hexagonal cell $a = b$ = 4.57 Å, γ = 113.5°, may be extracted (*27*) with the same area as that of the oblique cell of cadmium arachidate.

The d spacing of the strong peak at q_x = 0.799 Å^{-1} (d = 7.86 Å) is exactly twice that of the {1,0} reflection (q_x = 1.599 Å^{-1}, d = 3.93 Å, Fig. 3B). None of the other peaks has a d spacing that is an integral multiple of any of the "triplet" peaks. The plausible conjecture at this point is that the peak at q_x = 0.799 Å^{-1} arises from ordering of the Cd^{2+} ions commensurate with the arachidate lattice.

The question now is whether we can index all other peaks as fractional orders with respect to the arachidate lattice and thereby prove that the Cd and arachidate lattices are commensurate. This would require that the area of the Cd unit cell be n times that of the arachidate cell of 19.2 Å^2, where n must be an even number because the molar ratio of doubly charged cation Cd^{2+} to the singly charged carboxylate anion CO_2^- is 1:2, if all the head groups are fully ionized. On the assumption that the two observed peaks at q_x = 0.689 Å^{-1} (d = 9.11 Å) and q_x = 0.799 Å^{-1} (d = 7.86 Å)

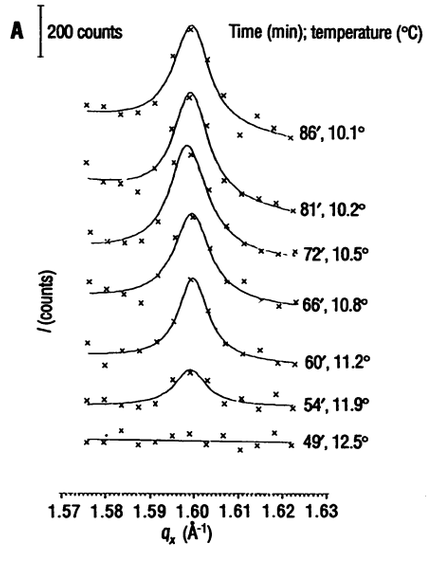

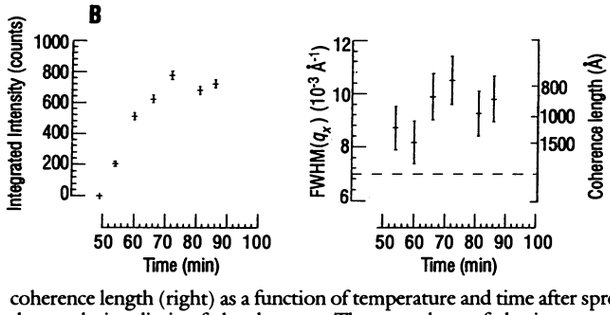

Fig. 2. Uncompressed monolayer of arachidic acid spread over a $CdCl_2$ subphase (10^{-3} M), pH = 8.8, at 9°C. The mean molecular area is 28 Å^2 with zero surface pressure. (**A**) GID profiles at q_x = 1.599 Å^{-1} as a function of temperature and time after spreading. Time and temperature are indicated for eachpeak. (**B**) Integrated intensity (left) and coherence length (right) as a function of temperature and time after spreading. The dashed line indicates the resolution limit of the detector. The error bars of the integrated intensities were derived from counting statistics. The errors bars (± SE) corresponding to the coherence lengths were derived from the curve-fitting analysis of the peaks.

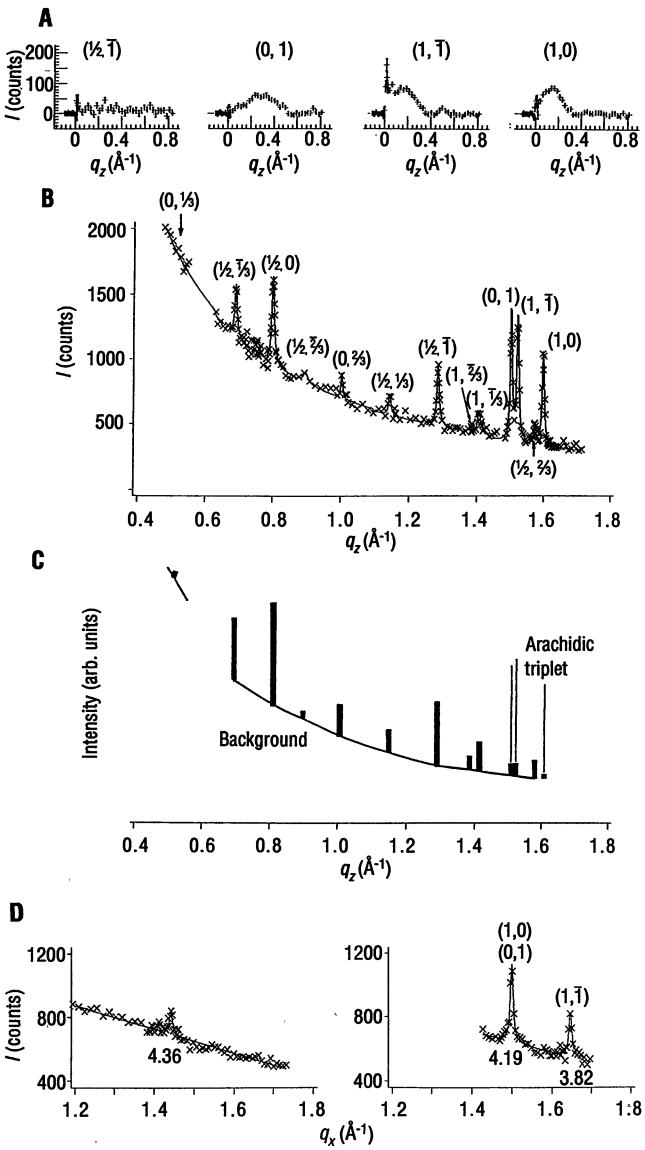

Fig. 3. Uncompressed arachidic acid monolayer spread over a $CdCl_2$ subphase (10^{-3} M), pH = 8.8, at 9°C. The mean molecular area was 28 Å^2 with zero surface pressure. (**A**) Bragg rod scans of the GID peaks in (B). (**B**) The observed GID powder pattern. The assigned (h,k) indices are indicated for each peak. (**C**) The calculated powder diffraction pattern for the Cd lattice. (**D**) GID measurements of arachidic acid spread over a pure water subphase at 9°C. (Left) Uncompressed monolayer, mean molecular area of 28 Å^2 with zero surface pressure. (Right) Compressed monolayer, surface pressure of 27 mN m^{-1}. The d spacing (in angstroms) and the assigned (h,k) indices are indicated below and above each peak, respectively.

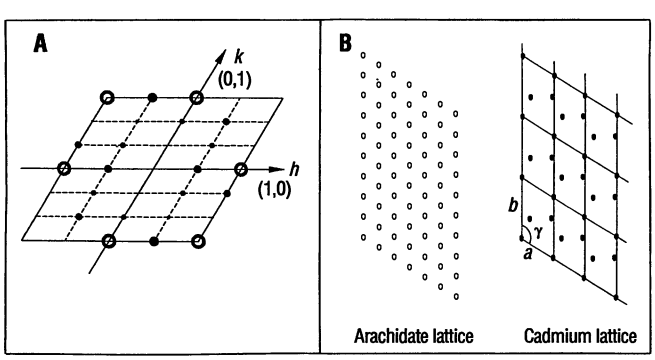

Fig. 4. (**A**) The reciprocal lattice with the areas of spots proportional to the corrected intensities. The open circles represent the reflections corresponding to the arachidate lattice, and the filled circles represent those corresponding to the Cd lattice. (**B**) (Left) Arachidate unit cell: a = 4.60 Å, b = 4.89 Å, γ = 121.3°, area = 19.2 Å^2. (Right) A 2 × 3 Cd unit cell: a = 9.19 Å, b = 14.67 Å, γ = 121.3°, area = 115.4 Å^2, with the three Cd positions corresponding to the best fit.

We may index all the observed reflections in terms of this supercell using indices $\{2h,3k\}$, so that the arachidate peaks index as $\{0,3\}$, $\{2,\bar{3}\}$, and $\{2,0\}$. We obtained precise dimensions of the supercell by least-squares fit, making use of all the observed 2θ peak positions and the derived h,k indices to yield a' = 9.19(1) Å, b' = 14.67(1) Å, γ' = 121.33(5)° (the number in parentheses is the estimated error of the last digit), with an average deviation $(2\theta_{obs} - 2\theta_{calc})$ for all reflections of 0.015°. Naturally, the arachidate cell is given by $a = (1/2)a'$ = 4.595(5) Å, $b = (1/3)b'$ = 4.890(3) Å, $\gamma = \gamma'$ = 121.33(5)°.

The shape of the Bragg rods proves unambiguously that the peaks of fractional order are due to a thin layer (of Cd^{2+} ions) and not to some superstructure of the arachidate molecules, such as a herringbone arrangement of the arachidate backbone planes (*28*). The observed intensities, corrected for crossbeam area (*6*) and Lorentz and polarization factors, are listed in Table 1 along with their estimated errors. The reciprocal lattice is presented in Fig. 4A. The observed $\{h,k\}$ reflections are shown as spots of area proportional to the corrected intensities. The unit cells in real space are shown in Fig. 4B. For the arachidate cell there is only one such molecule per unit cell; the 2 × 3 unit cell of Cd contains three such atoms.

To determine the positions of the Cd atoms in the unit cell, the origin of the cell is chosen to be on a Cd atom. The intensities calculated for all reflections are then fitted by least squares to the observed ones in Table 1, with the x,y positions of the remaining two Cd atoms used as fit variables. These two atoms were allowed to rove independently over the whole cell. We assign a root-mean-square in-plane vibrational amplitude of 0.7 Å to each Cd atom. Only one solution was obtained (*29*) for the Cd positions whose $[x,y]$ fractional coordinates are [0,0], [0.264(23),0.405(21)], and [−0.059(28),0.637(25)] (Fig. 4B). The errors (SE) in parentheses were derived from the least-squares fit. The three Cd^{2+} ions are not related by symmetry; thus the two-dimensional space group is $p1$ (*30*). The calculated powder pattern (Fig. 3C) fits the observed intensity data in Fig. 3B very well. The contributions from the Cd lattice at the arachidate "triplet" positions are smaller by about a factor of 10 than the total intensity. Because the two-dimensional space group of cadmium arachidate is $p1$, there are two enantiomorphous crystal structures thereof on the water surface, related to each other by mirror reflection (*31*).

Although the orientation of the arachidate lattice is found to be identical to that of the Cd lattice, the data may not allow for the

are reciprocal base vectors of the Cd unit cell, we can derive the angle between these two vectors for a given value of n. This angle then determines two possible orientations of the reciprocal vector at q_x = 0.689 Å^{-1} vis-à-vis the (1,0) reciprocal axis. Only for n = 6 does one of these two orientations yield components (0.5004,−0.3333) of this reciprocal vector that are consistent with fractional indices $\{1/2,-1/3\}$. We can then index all the remaining peaks with $\{h/2,k/3\}$ indexing as indicated in Table 1 and Fig. 3B. The Cd unit cell is thus a 2 × 3 supercell of the arachidate lattice. To satisfy charge neutrality there must be three Cd^{2+} ions per supercell.

Table 1. Observed and calculated x-ray powder diffraction data. Observed q_x values of the diffraction peaks, calculated d spacings and corresponding h,k indices, referred to the arachidate lattice, observed intensities (corrected for cross-sectional area, Lorentz and polarization factors) of the diffraction peaks and calculated intensities of the reflections from the Cd^{2+} ions only.

h	k	Observed intensity*	Calculated intensity	q_x (Å^{-1})	Calculated d spacing (Å)
		Reflections from Cd^{2+}			
0	1/3	<0.05 (5)	0.15	0.501	12.54
1/2	−1/3	0.84 (3)	0.85	0.689	9.11
1/2	0	1.70 (7)	1.73	0.799	7.86
1/2	−2/3	0.33 (15)	0.22	0.900	7.02
0	2/3	0.72 (20)	0.56	1.002	6.26
1/2	1/3	0.76 (20)	0.61	1.143	5.50
1/2	−1	2.63 (20)	2.30	1.284	4.89
1	−2/3	0.40 (20)	0.58	1.377	4.55
1	−1/3	1.37 (40)	1.28	1.406	4.47
1/2	2/3	1.36 (40)	1.07	1.573	3.99
		Reflections from arachidate and Cd^{2+}			
0	1	7.68		1.503	4.18
1	−1	8.13		1.523	4.13
1	0	6.15		1.599	3.93

*The estimated errors (in parentheses) represent an overall uncertainty with allowance for possible systematic errors.

determination of the displacement between them. This would require an accurate scaling of the two sets of structure factors and then the fitting of a phase factor in the sum of structure factors for coinciding reflections. Perhaps atom-atom potential energy calculations may also be used to obtain a relative fit between the two lattices.

In summary, the observed powder pattern comprising seven reflections from the Cd lattice, three fundamental reflections from the arachidate lattice, plus three higher order reflections from the latter (not shown here) is by far the richest spectrum ever observed from a Langmuir monolayer with the associated bound atoms. It proves the presence of an ordered layer of Cd^{2+} ions near the surface, of a unit cell sixfold larger than, and commensurate with, that of the arachidate monolayer. The positions of the Cd^{2+} ions within the unit cell could also be accurately determined. Issues requiring further research include the concentration of interleaving NH_3 and water molecules in the ionic layer, their role in inducing long-range order in the Cd^{2+} layer, and the determination of the displacement between the two lattices, which will involve a complete analysis of the Bragg rod profiles so as to provide information on the packing arrangement of the arachidate moiety.

REFERENCES AND NOTES

1. H. Kuhn and D. Möbius, *Angew. Chem.* **83**, 672 (1971).
2. L. Addadi and S. Weiner, *Proc. Natl. Acad. Sci. U.S.A.* **82**, 4110 (1985); L. Addadi, J. Moradian, E. Shai, N. G. Maroudas, S. Weiner, *ibid.* **84**, 2732 (1987).
3. E. M. Landau, R. Popovitz-Biro, M. Levanon, L. Leiserowitz, M. Lahav, *Mol. Cryst. Liq. Cryst.* **134**, 323 (1986); S. Mann, B. R. Heywood, S. Rajam, J. D. Birchall, *Nature* **334**, 692 (1988).
4. K. Kjaer, J. Als-Nielsen, C. A. Helm, L. A. Laxhuber, H. Möhwald, *Phys. Rev. Lett.* **58**, 2224 (1987); C. A. Helm, H. Möhwald, K. Kjaer, J. Als-Nielsen, *Biophys. J.* **52**, 381 (1987); S. Grayer Wolf *et al.*, *Nature* **328**, 63 (1987); S. Grayer Wolf *et al.*, *Science* **242**, 1286 (1988).
5. P. Dutta *et al.*, *Phys. Rev. Lett.* **58**, 2228 (1987).
6. J. Als-Nielsen and K. Kjaer, in *Proceedings of the NATO Advanced Study Institute, Phase Transitions in Soft Condensed Matter* (Geilo, Norway, 4 to 14 April 1989), T. Riste and D. Sherrington, Eds. (Plenum, New York, 1989), pp. 113–137.
7. L. Bosio, J. J. Benatar, F. Rieutord, *Rev. Phys. Appl.* **22**, 775 (1987); R. M. Richardson and S. J. Roser, *Liquid Cryst.* **2**, 797 (1987); K. Kjaer, J. Als-Nielsen, C. A. Helm, P. Tippman-Krayer, H. Möhwald, *J. Phys. Chem.* **93**, 3200 (1989).
8. Recently, we presented indirect evidence from GID data in favor of an ordered layer of monovalent K^+ ions bound to the anionic (CO_2^-) group of an α–amino acid monolayer at high pH in both the uncompressed and the compressed state (*9*).
9. D. Jacquemain *et al.*, *J. Am. Chem. Soc.* **112**, 7724 (1990).
10. M. J. Bedzyk, G. M. Bommarito, M. Caffrey, T. L. Penner, *Science* **248**, 52 (1990).
11. J. M. Bloch *et al.*, *Phys. Rev. Lett.* **61**, 2941 (1988).
12. For the GID measurements, we used a linear position-sensitive detector (PSD) mounted vertically behind a horizontally collimating Soller slit. For measurements carried out on the wiggler beam line W1 and on the bending magnet beam line D4, the synchrotron beam was monochromated by Bragg reflection from a Ge(111) crystal to a wavelength λ = 1.40 and 1.38 Å, respectively. The GID angle of incidence was 0.85 α_c, where $\alpha_c = 0.138°$ is the critical angle for total external reflection. The dimensions of the footprint of the incoming x-ray beam on the surface were 50 by 5 mm (Fig. 1).
13. Spreading solutions of arachidic acid (Fluka, purity ≥99%) were prepared in chloroform (Merck, analytical grade). Millipore purified water (resistivity ρ ≤ 0.05 μS) was used. The subphase composition and pH were varied with NH_3 (British Drug Houses, analytical grade) and $CdCl_2$ (Merck, analytical grade). The pH of about 8.8 was the maximum we were able to obtain without inducing precipitation. At higher pH a fine white powder precipitates from the solution; its x-ray pattern is presently being analyzed.
14. The symbols q_x and q_z are the in-plane and out-of-plane components, respectively, of the scattering wave vector $\mathbf{q}$: $q_x \sim (4\pi/\lambda)\sin\theta$, where 2θ is the horizontal scattering angle, and $q_z = (2\pi/\lambda)\sin\alpha_f$, where α_f is the angle between the diffracted wave and the subphase surface (Fig. 1).
15. S. W. Barton *et al.*, *J. Chem. Phys.* **89**, 2257 (1988).
16. T. M. Bohanon, B. Lin, M. C. Shih, G. E. Ice, P. Dutta, *Phys. Rev. Lett.* **65**, 19 (1990).
17. R. M. Kenn *et al.*, *J. Phys. Chem.* **95**, 2092 (1991).
18. For a measured diffraction peak of the width FWHM(q_x) (denoting the full width at half maximum), the resolution-corrected width is $W = [\mathrm{FWHM}(q_x)^2 - \Delta(q_x)^2]^{1/2}$, where $\Delta(q_x)$ is the resolution of the Soller slit of width 0.007 Å^{-1}. By the Debye-Scherrer formula (*19*), the width W corresponds to a coherence length $L = 0.90 \times 2\pi/W$.
19. A Guinier, *X-ray Diffraction* (Freeman, San Francisco, 1968), p. 121.
20. The intensities of the q_x scans of Fig. 3A are integrated over a vertical wave vector range q_z from 0 to 1 Å^{-1}. Scanning the PSD through a particular q_x reflection yields the q_z distribution of that reflection, the so-called Bragg rod.
21. R. Feidenhans'l, *Surf. Sci. Rep.* **10**, 3, 105 (1989).
22. D. Jacquemain *et al.*, *J. Phys. (Paris) Colloq. 50* (suppl. 10), colloque C7, 29 (1989).
23. If we extrapolate the Bragg rod intensity profile of the reflection at $q_x = 1.284$ Å^{-1}, it does not drop to half its maximum before, say, $q_z = 1.2$ Å^{-1}; then we can deduce (*22*) that the thickness is $\leq 2\pi/2 \times 1.2 \sim 2.5$ Å.
24. We recorded the Bragg rods of the two observed peaks at $q_x = 0.689$ and 0.799 Å^{-1} at beam line D4, using another sample (with a subphase pH of 8.6); therefore, they do not appear in Fig. 3A. Nevertheless, their profiles are very similar to that measured at $q_x = 1.284$ Å^{-1} (shown in Fig. 3A). Both the extension of the Bragg rods along q_z and the sharpness in q_x of the peaks rule out the possibility that the peaks are due to three-dimensional crystallites in the aqueous subphase, for example, such as the white powder precipitate (*13*) at pH values >8.8.
25. Bragg rod intensity profiles are modulated by the molecular x-ray structure factor of the diffracting amphiphilic molecules and give precise information on the molecular orientation in the two-dimensional crystal (*6, 22*). If the aliphatic tails are uniformly and rigidly tilted in the monolayer, the angle t between the molecular axis and the surface normal is given by (*6, 22*):
$$\cos\psi_{hk} \tan t = q_z^0 / |\mathbf{G}_{hk}|$$
where q_z^0 is the position of the maximum along the Bragg rod, and ψ_{hk} is the azimuthal angle between the tilt direction projected on the xy plane and of $\mathbf{G}_{hk}$. $\mathbf{G}_{hk} = 2\pi(h\mathbf{a}^* + k\mathbf{b}^*)$, where $\mathbf{a}^*$ and $\mathbf{b}^*$ are the reciprocal lattice vectors, and h and k are the integer components of the corresponding lattice point. The molecules will therefore be perpendicular to the surface when, for all reflections (h,k), q_z^0 tends to 0 Å^{-1}. The Bragg rod profiles of all three arachidate reflections peak at $q_z \sim 0.2$ to 0.3 Å^{-1}, which are far removed from the horizon at $q_z = 0$ Å^{-1}. Thus, the molecule does not tilt in either the (0,1), (1,$\bar{1}$), or (1,0) plane. We have deduced from analysis of the Bragg rod data the tilt direction and orientation of the arachidate molecule with respect to the unit cell (F. Leveiller *et al.*, in preparation).
26. For coinciding reflections (h,k) and $(\bar{h},\bar{k})$, we use the symbol $\{h,k\} = (h,k)$ and $(\bar{h},\bar{k})$.
27. For a more obvious comparison with the distorted hexagonal cell of compressed arachidic acid over pure water we may describe the oblique cell of the arachidate moiety of cadmium arachidate via the transformation $\mathbf{a}' = \mathbf{a} + \mathbf{b}$, $\mathbf{b}' = -\mathbf{a}$ yielding $a' = 4.654(4)$ Å, $b' = 4.595(5)$ Å, $\gamma' = 116.3°$. These precise dimensions were derived by least squares as described later in the text. The cell obtained for compressed arachidic acid over pure water is similar to that obtained by Bohanon *et al.* (*16*) for compressed films of $C_{20}H_{41}CO_2H$ at 5°C over pure water and by Kenn *et al.* (*17*) for compressed $C_{21}H_{43}CO_2H$ at 7°C: The unit cell is a distorted hexagonal $a = b = 4.49$ Å, $\gamma = 112°$, area = 18.7 Å^2, more properly described (*16*) as centered rectangular $a' = 7.46$ Å, $b' = 5.01$ Å.
28. E. Von Sydow, *Acta Crystallogr.* **8**, 557 (1955); *Ark. Kemi* **9**, 231 (1956).
29. The low range in q_x (0.5 Å$^{-1} \leq q_x \leq 1.6$ Å^{-1}) does not allow for a precise determination of the root-mean-square in-plane vibrational amplitude because a value of 0.6 Å also gave as good a fit to the data.
30. However, the positions of the three Cd^{2+} ions in the

Cd unit cell do indicate some tendency toward twofold symmetry, namely, space group $p2$.

31. We shall attempt to observe such enantiomorphism by epifluorescence microscopy. V. Von Tscharner and H. M. McConnel, *Biophys. J.* **36**, 409 (1981); M. Lösche and H. Möhwald, *Rev. Sci. Instrum.* **55**, 1968 (1984); G. B. Moore, C. M. Knobler, S. Akamatsu, F. Rondelez, *J. Phys. Chem.* **94**, 4588 (1990).

32. We thank C. Böhm and R. Kenn for assistance during the experiments, H. Möhwald for helpful discussions, A. Yonath for use of laboratory facilities at the Max Planck Unit for Structural Molecular Biology, and R. Feidenhans'l for help in the fitting analysis. Supported by the U.S.–Israel Binational Science Foundation, Jerusalem; the Petroleum Fund of the American Chemical Society; the German Israeli Foundation; the Fund for Basic Research of the Israel Academy of Science and Humanities; and the Danish Foundation for Natural Sciences. We thank Hasylab, DESY, Hamburg, for beam time.

2 November 1990; accepted 8 March 1991

Satellite Observations of Smoke from Oil Fires in Kuwait

S. S. LIMAYE, V. E. SUOMI, C. VELDEN, G. TRIPOLI

Extensive dark smoke clouds associated with burning oil wells in Kuwait have been seen in data from weather satellites since early February 1991. The smoke is dispersed over a wide area. Variable and strong low level winds have held most of the smoke plume below 3 to 5 kilometers within a few hundred kilometers of the source. Thin veils of smoke have been detected in METEOSAT data as far away as 2000 kilometers east of Kuwait, over southwestern Pakistan at heights between 6 and 7 kilometers. The occasional presence of convective clouds over the fires indicates that some scavenging of the smoke is taking place.

SINCE EARLY FEBRUARY 1991, EXTENSIVE smoke clouds associated with burning oil wells in Kuwait have been seen in NOAA-10 and NOAA-11 polar orbiting satellite observations (*1*). Visible imagery from these and the METEOSAT geosynchronous satellite shows that the smoke plumes are quite dark (albedo generally <8%). At night the 0.84-μm channel on the polar satellites clearly shows a glow associated with the six isolated burning oil fields. The local impact of the smoke has been noted in media reports (*2*).

Before the ignition of the oil wells, several concerns were raised that the resulting smoke could have significant impact on climate by virtue of its ability to absorb sunlight over a large area (*3*). An essential element of these is that the smoke be lofted high in the atmosphere. A recent, more specific analysis of the fires in Kuwait suggests that the likely impacts on climate are small (*4*). The observations to date suggest that most of the smoke has been restricted to the lower atmosphere (≲3 km) within ~1000 km of the source; however, some smoke has been detected at an altitude of 6 to 7 km nearly 2000 km from the source. Here we report on satellite observations of the dispersal of smoke from these fires over a larger region, estimates of the altitudes at which the smoke is detectable, and some interaction of the smoke with the transient synoptic weather patterns. As the regional weather is dynamic and seasonal, these observations should be viewed as illustrative, but provide an indication of the need for future monitoring.

Figure 1 shows the horizontal extent of the smoke as observed on 4 March 1991 in one solar (0.84 μm) and two infrared spectral bands (3.7 and 10.9 μm) from the NOAA-10 AVHRR sensor (*1*). The smoke cloud typically appears in the two short wavelength channels as dark plumes extending from four major fields in southern Kuwait (Fig. 1A) and from two fields north of Kuwait City (obscured by the high-level cirrus clouds in Fig. 1A). These sunlight-absorbing plumes were detectable over an area as much as 42,000 km^2, while the optically thicker region (optical thickness of about 2) blanketed an area as much as 7,100 km^2. On other days, relatively thin veils of smoke have been detected over a much larger area, nearly 180,000 km^2, such as on 18 March 1991. The coastline south of Kuwait City is completely obscured in the 0.6-μm channel (not shown) and can be seen just barely in the 0.84-μm data. Smoke plumes can be traced as light bands (lower brightness temperatures) to six clusters, the largest of which is south of Kuwait City [Burgan oil field, 210 wells (*4*)]. The average optical thickness of the smoke at 0.6 μm over the darkest parts is estimated to about 2, but varies with the ambient conditions and distance from the source. The smoke is typically detectable over the desert (high visible albedo) at optical thicknesses as low as about 0.2 from the visible data by its contrast and drift in time-lapse images but is not usually unambiguously detectable over water (low visible albedo) from satellite observations at either visible or infrared wavelengths.

The size of the particles and the heights to which they can rise are key factors that determine the extent of the areal spread, atmospheric residence times, and hence the degree of impact on weather or climate. The satellite observations present some information about both of these smoke characteristics. Small particles (comparable to the visible wavelengths) absorb sunlight but not the long wave thermal radiation emitted by the earth.

An indication of the average particle size is provided by the appearance of the smoke at different wavelengths. At visible wavelengths the smoke is dark; it is relatively transparent at 3.7 μm (Fig. 1B) and more so at 10.9 μm (Fig. 1C). The west shore of the Persian Gulf can be clearly seen at the longer wavelengths. These observations suggest that the smoke particles are predominantly smaller than about 1 μm, although some larger sized particles are also present, consistent with the expected size of the soot particles produced from oil fires (*5, 6*). However, the long wave transparency of the smoke within a few tens of kilometers of the source varies from day to day and also as a function of time of day. Satellite observations indicate that variations in the number density of the smoke particles and in the particle size distribution likely have resulted in variations (more larger particles) in the ambient atmospheric conditions and the amount of accompanying water vapor (because of the intrusion of water into the oil wells and as a combustion product and condensation onto the smoke particles). These are indicated by increased opacity at 3.7 and 10.9 μm, as well as by the appearance of water (white) clouds within the smoke plume in the visible images and supported by reports of black rain (*2*).

Height determination is the most difficult to achieve from satellite observations at visible wavelengths, but measurements of smoke drift, cloud shadows, and stereoscopic separation allow some estimates to be made. An indication of the relative level of the smoke plume is given by a few high-level clouds over the gulf that can be seen to cast shadows to the west onto the lower level smoke deck (Fig. 1A). The heights of small clouds over the smoke plume in the gulf region as estimated from their shadows are approximately 7 to 9 km. Nearby conventional upper air data (Shiraz, Iran) suggests that the clouds are at an approximate alti-

S. S. Limaye, V. E. Suomi, C. Velden, Space Science and Engineering Center, University of Wisconsin–Madison, 1225 West Dayton Street, Madison, WI 53706.
G. Tripoli, Department of Meteorology, University of Wisconsin–Madison, Madison, WI 53706.